ARMY RESEARCH LABORATORY

ARL

Numerical Investigation of Supersonic Base Flow With Base Bleed

Jubaraj Sahu
Karen R. Heavey

ARL-TR-955   December 1995

19960227 016

DTIC QUALITY INSPECTED 1

NOTICES

Destroy this report when it is no longer needed. DO NOT return it to the originator.

Additional copies of this report may be obtained from the National Technical Information Service, U.S. Department of Commerce, 5285 Port Royal Road, Springfield, VA 22161.

The findings of this report are not to be construed as an official Department of the Army position, unless so designated by other authorized documents.

The use of trade names or manufacturers' names in this report does not constitute indorsement of any commercial product.

REPORT DOCUMENTATION PAGE

Form Approved
OMB No. 0704-0188

Public reporting burden for this collection of information is estimated to average 1 hour per response, including the time for reviewing instructions, searching existing data sources, gathering and maintaining the data needed, and completing and reviewing the collection of information. Send comments regarding this burden estimate or any other aspect of this collection of information, including suggestions for reducing this burden, to Washington Headquarters Services, Directorate for Information Operations and Reports, 1215 Jefferson Davis Highway, Suite 1204, Arlington, VA 22202-4302, and to the Office of Management and Budget, Paperwork Reduction Project(0704-0188), Washington, DC 20503.

1. AGENCY USE ONLY *(Leave blank)*	2. REPORT DATE	3. REPORT TYPE AND DATES COVERED
	December 1995	Final, September 1994 - October 1995

4. TITLE AND SUBTITLE

Numerical Investigation of Supersonic Base Flow With Base Bleed

5. FUNDING NUMBERS

PR: 1L161102AH43

6. AUTHOR(S)

Jubaraj Sahu and Karen R. Heavey

7. PERFORMING ORGANIZATION NAME(S) AND ADDRESS(ES)

U.S. Army Research Laboratory
ATTN: AMSRL-WT-PB
Aberdeen Proving Ground, MD 21005-5066

8. PERFORMING ORGANIZATION REPORT NUMBER

ARL-TR-955

9. SPONSORING/MONITORING AGENCY NAMES(S) AND ADDRESS(ES)

10. SPONSORING/MONITORING AGENCY REPORT NUMBER

11. SUPPLEMENTARY NOTES

12a. DISTRIBUTION/AVAILABILITY STATEMENT

Approved for public release; distribution is unlimited.

12b. DISTRIBUTION CODE

13. ABSTRACT *(Maximum 200 words)*

A zonal, implicit, time-marching Navier-Stokes computational technique has been used to compute the turbulent supersonic base flow over a cylindrical afterbody with base bleed. A critical element of calculating such flows is the turbulence model. Two eddy viscosity turbulence models have been used in the base region flow computations. These models include an algebraic turbulence model and a two-equation k-ϵ model. The k-ϵ equations are solved using an implicit algorithm, and calculations with the k-ϵ model are extended up to the wall. Flow field computations have been performed for a cylindrical afterbody at $M = 2.46$ and at an angle of attack of $\alpha = 0$. The results are compared to the experimental data for the same conditions and the same configuration. Details of the mean flow field as well as the turbulence quantities have been presented. In addition, the computed base pressure distribution has been compared with the experiment. In general, the k-ϵ turbulence model performs better in the near wake than the algebraic model and predicts the base pressure much better.

14. SUBJECT TERMS

base flow, base bleed, turbulence, modeling, supersonic

15. NUMBER OF PAGES

33

16. PRICE CODE

17. SECURITY CLASSIFICATION OF REPORT	18. SECURITY CLASSIFICATION OF THIS PAGE	19. SECURITY CLASSIFICATION OF ABSTRACT	20. LIMITATION OF ABSTRACT
UNCLASSIFIED	UNCLASSIFIED	UNCLASSIFIED	SAR

NSN 7540-01-280-5500

Standard Form 298 (Rev. 2-89)
Prescribed by ANSI Std. 239-18   298-102

INTENTIONALLY LEFT BLANK.

TABLE OF CONTENTS

INTENTIONALLY LEFT BLANK.

LIST OF FIGURES

INTENTIONALLY LEFT BLANK.

1. INTRODUCTION

One of the important parameters in the design of a shell is the total aerodynamic drag. The total drag consists of three drag components: the pressure drag or the wave drag (excluding the base), the viscous drag, and the base drag. The base drag component is a large part of the total drag and can be as high as 50% or more of the total drag. Of the three drag components, the most difficult one to predict is the base drag. The base drag depends on the pressure acting on the base. Therefore, it is necessary to predict the base pressure as accurately as possible.

The ability to compute the base region flow field for projectile configurations using Navier-Stokes computational techniques has been developed over the past few years.[1,2,3] Recently, improved numerical predictions have been obtained using a more advanced zonal upwind flux-split algorithm.[4,5] This zonal scheme preserves the base corner and allows better modeling of the base region flow. These studies have included base flows for different base geometries. This capability is very important for determining aerodynamic coefficient data including the total aerodynamic drag. As indicated earlier, a number of base flow calculations have been made, and base drag and total drag have been predicted with reasonable accuracy. However, due to the lack of available data, the predictive capabilities were not assessed earlier with detailed base pressure distributions, mean flow velocity components, and turbulence quantities. This is especially true of base flow for axisymmetric bodies at transonic and supersonic speeds. Recently, experimental measurements have been made in the base region for supersonic flow over a cylindrical afterbody without base bleed.[6] The data included base pressure distribution (along the base), mean flow, and turbulence quantities. Numerical computations[7] were made for this case, and computed results were compared with this data. The detailed experimental data were critical in validating the computational results, especially for the turbulence modeling and grid resolution issues.

Figure 1 is a schematic diagram showing the important features of supersonic base flow with base bleed. The approaching supersonic turbulent boundary layer separates at the base corner, and the free shear layer region is formed in the wake. The flow expands at the base corner and is followed by the recompression shock downstream of the base, which realigns the flow. The flow then redevelops in the trailing wake. In the absence of base bleed, a low-pressure region is formed immediately downstream of the base, which is characterized by a low-speed recirculating flow region. Interaction between this recirculating region and the inviscid external flow occurs through the free

shear mixing region. This is the region where turbulence plays an important role. Injection of low-speed air into the base region displaces the entire recirculation region downstream into the wake. The bleed flow fills in the near wake region. This, in turn, weakens the recompression shock, resulting in an increase of base pressure or a reduction in base drag.

The drag reduction due to base bleed at supersonic speeds is of practical importance. The effect of base bleed or mass injection has been studied experimentally.[8-10] These early experiments involved cold and hot gas injection for cylindrical and boat-tailed afterbodies and clearly showed the effectiveness of base bleed on base pressure. Most of these experimental investigations were rather limited in nature and lacked measurements of detailed base pressure and near wake flow field such as mean flow and turbulence quantities. Such detailed experimental data have been recently available[11] for supersonic flow over a cylindrical afterbody with base bleed. This set of experimental data not only provides insight into the details of the fluid dynamic interactions in the near wake but also serves as a benchmark for validation of computational results. This paper describes the computational investigation of supersonic base flow with base bleed for the same experimental model and conditions.

The basic configuration used in this study is a cylindrical afterbody. As mentioned earlier, a simple composite grid scheme has been used for accurate modeling of the base corner. Numerical flow field computations have been performed at M_∞= 2.46 and at a 0° angle of attack. Two turbulence models (an algebraic model and a two-equation model) are used in the base flow region. All the computations have been performed on the Cray Y-MP supercomputer. Details of the flow field such as Mach number contours and base pressure distributions are presented. Computed base pressure distributions are compared with available experimental data for the same conditions and the same configuration.

2. GOVERNING EQUATIONS AND SOLUTION TECHNIQUE

The complete set of time-dependent, Reynolds-averaged, thin-layer Navier-Stokes equations is solved numerically to obtain a solution to this problem. The numerical technique used is an implicit, finite-difference scheme. Although time-dependent calculations are made, the transient flow is not of primary interest at the present time. The steady flow, which is the desired result, is obtained in a time asymptotic fashion.

2.1 Governing Equations

The complete set of three-dimensional (3-D), time-dependent, generalized geometry, Reynolds-averaged, thin-layer, Navier-Stokes equations for general spatial coordinates ξ, η, and ζ can be written as follows:[12]

$$\partial_\tau \hat{q} + \partial_\xi \hat{F} + \partial_\eta \hat{G} + \partial_\zeta \hat{H} = Re^{-1} \partial_\zeta \hat{S},$$ (1)

where

$\tau = t$ - time,

$\xi = \xi(x, y, z, t)$ - longitudinal coordinate,

$\eta = \eta(x, y, z, t)$ - circumferential coordinate,

$\zeta = \zeta(x, y, z, t)$ - nearly normal coordinate.

In Equation 1, $\hat{q}$ contains the dependent variables, and $\hat{F}$, $\hat{G}$, and $\hat{H}$ are flux vectors. The thin-layer approximation is used here, and the viscous terms involving velocity gradients in both the longitudinal and circumferential directions are neglected. The viscous terms are retained in the normal direction, ζ, and are collected into the vector $\hat{S}$. These viscous terms are used everywhere. However, in the wake or the base region, similar viscous terms are also added in the streamwise direction. For this computation, the diffusion coefficients μ and κ contain molecular and turbulent parts. The turbulent contributions are supplied through either algebraic or a two-equation k-ϵ turbulence model.

2.2 Numerical Technique

The implicit, approximately factored scheme for the thin-layer Navier-Stokes equations using central differencing in the η and ζ directions and upwinding in ξ is written in the following form:

3

$$\left[I + h\delta_\xi^b (\hat{A}^+)^n + h\delta_\zeta \hat{C}^n - hRe^{-1}\bar{\delta}_\zeta J^{-1}\hat{M}^n J - D_i|_\zeta \right]$$

$$\times [I + h\delta_\xi^f (\hat{A}^-)^n + h\delta_\eta \hat{B}^n - D_i|_\eta]\Delta \hat{Q}^n$$

$$= -\Delta t\{\delta_\xi^b [(\hat{F}^+)^n - \hat{F}_\infty^+] + \delta_\xi^f [(\hat{F}^-)^n - \hat{F}_\infty^-] + \delta_\eta (\hat{G}^n - \hat{G}_\infty)$$

$$+ \delta_\zeta (\hat{H}^n - \hat{H}_\infty) - Re^{-1}\bar{\delta}_\zeta (\hat{S}^n - \hat{S}_\infty)\} - D_e(\hat{Q}^n - \hat{Q}_\infty) ,$$

(2)

where $h = \Delta t$ or $(\Delta t)/2$ and the free stream base solution is used. Here, δ is typically a three-point second-order accurate central difference operator, $\bar{\delta}$ is a midpoint operator used with the viscous terms, and the operators δ_ξ^b and δ_ξ^f are backward and forward three-point difference operators. The flux $\hat{F}$ has been eigensplit, and the matrices $\hat{A}$, $\hat{B}$, $\hat{C}$, and $\hat{M}$ result from local linearization of the fluxes about the previous time level. Here, J denotes the Jacobian of the coordinate transformation. Dissipation operators D_e and D_i are used in the central space differencing directions. The smoothing terms used in the present study are of the form:

$$D_e|_n = (\Delta t) J^{-1}\left[\epsilon_2 \bar{\delta}\rho(B)\beta\bar{\delta} + \epsilon_4 \bar{\delta}\frac{\rho(B)}{1+\beta}\bar{\delta}^3\right]\Big|_n J ,$$

$$D_i|_n = (\Delta t) J^{-1}\left[\epsilon_2 \bar{\delta}\rho(B)\beta\bar{\delta} + 2.5\epsilon_4 \bar{\delta}\rho(B)\bar{\delta}\right]\Big|_n J ,$$

where

$$\beta = \frac{|\bar{\delta}^2 P|}{|(1+\delta^2)P|}$$

and where $\rho(B)$ is the true spectral radius of B. The idea here is that the fourth difference will be tuned down near shocks (e.g., as β gets large, the weight on the fourth difference drops down while the second difference tunes up).

4

2.3 Boundary Conditions

For simplicity, most of the boundary conditions have been imposed explicitly.[3] An adiabatic wall boundary condition is used on the body surface, and the no-slip boundary condition is used at the wall. The pressure at the wall is calculated by solving a combined momentum equation. Free stream boundary conditions are used at the inflow boundary as well as at the outer boundary. A symmetry boundary condition is imposed at the circumferential edges of the grid, while a simple extrapolation is used at the downstream boundary. A combination of symmetry and extrapolation boundary condition is used at the center line (axis). Since the free stream flow is supersonic, a nonreflection boundary condition is used at the outer boundary. The flow field is initially set to free stream conditions everywhere and then advanced in time until a steady-state solution is obtained.

For the base bleed case, boundary conditions are imposed at the bleed exit which include the total temperature and total pressure of the bleed gas as well as a mass injection parameter, I. The amount of bleed or gas injection is usually defined in terms of the mass injection parameter, $I = \dot{m}_j / \rho_\infty u_\infty A_b$, where m_j is the mass flow at the bleed exit and A_b is the area at the base. All dependent flow variables can be determined from these three quantities for the mass injection or base bleed case. The total pressure and temperature of injected gas are assumed to be constant at the bleed exit.

2.4 Composite Grid Scheme

In the present work, a simple composite grid scheme has been used where a large single grid is split into a number of smaller grids so that computations can be performed on each grid separately.[5] These grids use the available core memory one grid at a time. The remaining grids are stored on an external disk storage device. Some of today's supercomputers have a large incore memory to fit the large single grid. However, for accurate geometric modeling of complex projectile configurations which include blunt noses, sharp corners, and base cavities, it is also desirable to split the large database into a few smaller zones. The use of a composite grid scheme requires special care in storing and fetching the interface boundary data (i.e., the communication between the various zones). In the present scheme, there is a one-to-one mapping of the grid points at the interface boundaries. Thus, no interpolations are required. Details of the data storage, data transfer, and

5

other pertinent information such as metric and differencing accuracy at the interfaces can be found in the work of Sahu and Steger[4] and Sahu and Nietubicz.[5]

2.5 Turbulence Modeling

For the base flow calculations, two turbulence models have been used. The first one is an algebraic eddy viscosity model (Baldwin-Lomax model). The other one is a two- equation k-ε turbulence model which is also an eddy viscosity model.

2.5.1 Baldwin-Lomax Model

This model is the one developed by Baldwin and Lomax.[13] It is a two-layer model in which an eddy viscosity is calculated for an inner and an outer region. The inner region follows the Prandtl-Van Driest formulation. In both the inner and outer formulations, the distribution of vorticity is used to determine the length scales, thereby avoiding the necessity of finding the outer edge of the boundary layer. For the inner region,

$$(\mu_t)_{inner} = \rho \ell^2 |\omega| , \tag{3}$$

where

$$\ell = \kappa y [1 - \exp(-y^+ / A^+)]$$

$$y^+ = (\rho_w u_\tau y) / \mu_w , \quad u_\tau = \sqrt{(\tau_w / \rho_w)} ,$$

and $|\omega|$ is the absolute magnitude of vorticity. The eddy viscosity for the outer region is given by

$$(\mu_t)_{outer} = K C_{cp} \rho F_{wake} F_{kleb} (y) , \tag{4}$$

where $F_{wake} = y_{max} F_{max}$ or $C_{wk} y_{max} u_{dif}^2 / F_{max}$, the smaller of the two values. The quantities y_{max} and F_{max} are determined from the function $F(y) = y \omega [1 - exp(-y^+ / A^+)]$, where F_{max} is the maximum value of $F(y)$ and y_{max} is the value of y at which it occurs. The function F_{kleb} (y) is the Klebanoff intermittency factor. The quantity u_{dif} is the difference between the maximum and minimum total velocity in the profile, and, for boundary layers, the minimum is zero.

The outer formulation can be used in wakes as well as in attached and separated boundary layers. For free-shear layer flow regions or wakes, the Van Driest damping term $[exp(-y^+ / A^+)]$ is neglected. Also, for the base or wake region, the distance y is measured from the center line of symmetry. It is necessary to specify the following constants: $A^+ = 26$, $C_{cp} = 1.6$, $C_{kleb} = 0.3$, $C_{wk} = 0.25$, $\kappa = 0.4$, and $K = 0.0168$. This type of simple model is generally inadequate for complex flows containing flow separation regions such as base flow since it depends only on local information. The two-equation model contains less empiricism and allows the flow history to be taken into account.

2.5.2 Two-Equation k-ε Model

The two-equation turbulence model used here is Chien's k-ε model[14] which is similar to that of Jones and Launder.[15] In this model, two transport equations are solved for the two variables, k (turbulent kinetic energy) and ε (turbulent dissipation rate).

$$\rho \frac{Dk}{Dt} = \frac{\partial}{\partial X_j}\left[\left(\frac{\mu_t}{\sigma_k} + \mu\right)\frac{\partial k}{\partial X_j}\right] + \mu_t \frac{\partial u_i}{\partial X_j}\left(\frac{\partial u_i}{\partial X_j} + \frac{\partial u_j}{\partial X_i}\right)$$

$$- \rho\epsilon - 2\mu\frac{k}{y_n^2}$$

$$\rho \frac{D\epsilon}{Dt} = \frac{\partial}{\partial X_j}\left[\left(\frac{\mu_t}{\sigma_\epsilon} + \mu\right)\frac{\partial \epsilon}{\partial X_j}\right] + c_1\mu_t\frac{\epsilon}{k}\frac{\partial u_i}{\partial X_j}\left(\frac{\partial u_i}{\partial X_j} + \frac{\partial u_j}{\partial X_i}\right)$$

$$- c_2\rho\frac{\epsilon^2}{k} - 2\mu\frac{\epsilon}{y_n^2}e^{-y^+/2} \quad .$$

(5)

Here, y_n is the distance normal to the surface. The coefficients in the k and ϵ equations are given by

7

$$c_1 = 1.44$$

$$c_2 = 1.92\,[\,1 - 0.3\exp(-R_t^2)\,]$$

$$\sigma_k = 1.0\,, \quad \sigma_\epsilon = 1.3$$

$$c_\mu = 0.09\,[\,1 - \exp(-0.01\,y^+)\,]\ ,$$

where $R_t = k^2/\nu\epsilon$. The k-ϵ model employs the eddy viscosity concept and relates the turbulent eddy viscosity to k and ϵ by

$$\mu_t = c_\mu\rho(k^2/\epsilon)\,. \tag{6}$$

Following the same procedure used for the mean flow equations, the turbulence field equations are written in conservation form and then transformed into generalized coordinates.[16]

3. MODEL GEOMETRY AND EXPERIMENT

The computational accuracy of a numerical scheme can be established through comparisons with available experimental data. The model used in the experiment and in the computational study is shown in Figure 2. It is an axisymmetric cylindrical afterbody which has a diameter of 63.5 mm and a base bleed jet exit diameter of 25.4 mm. This figure also shows the location of the static pressure taps where base pressure was measured. The same configuration is used in the numerical simulations for a direct comparison.

Experimental measurements for this model have been made at the University of Illinois Supersonic Wind Tunnel[11] which was specifically designed for the study of axisymmetric base flows. The model was tested at a 0° angle of attack, Mach number of 2.46, and Reynolds number of 5.21 × 10^7 per meter. In addition to measuring the velocity components at a number of selected longitudinal positions in the wake or base region, the base pressure was measured at 10 positions along the base. Such detailed base pressure measurements have not been made in the past for the base bleed condition and are very helpful in the code validation process. The velocity profile is also

8

measured at a station upstream of the base, which provides the upstream boundary condition for base region flow field calculations.

4. RESULTS

Numerical computations have been made for the cylindrical afterbody at a Mach number of 2.46 and at a 0° angle of attack. The three-plane version of the 3-D code was run for the 0° angle of attack case. Two end planes were used to specify symmetric boundary conditions in the circumferential plane.

The solution technique requires the discretization of the entire flow region of interest into a suitable computational grid. The grid outer boundary has been placed 1 diameter away from the surface of the afterbody. The downstream boundary was placed 10 diameters away from the base. Since the calculations are in the supersonic regime, the computational outer boundary was placed close to the body, and a nonreflection boundary condition was used at that boundary. Figure 3 shows an expanded view of the grid in the base region. The surface points on the afterbody and the base were obtained first. These points were then used as inputs for obtaining the full grid using an algebraic grid generation program. The full grid is split into two zones, one upstream of the base, and the other one in the base region or the wake. These grids consist of 22×60 and 94×119 grid points, respectively. Figure 3 shows the longitudinal grid clustering near the base corner. Grid points are also clustered near the afterbody surface to capture the viscous effects in the turbulent boundary layer. This clustered grid points are spread out downstream of the base in the wake to capture the free shear layer region. As a part of grid resolution study, two other grids were considered. One was a coarse grid with half as many grid points, and the other one was a fine grid consisting of twice as many grid points as the original grid described above. For the 0° angle of attack case considered, the grid was rotated circumferentially 5° on either side of the midplane. This provided the three planes needed in the code to use central finite differences in the circumferential direction. In each case, the solution was marched from free stream conditions everywhere until the final converged solution was obtained. The results are now presented for both mean and turbulence quantities. Comparison of the computed results are made with the available experimental data.[11]

A few qualitative results are presented next. Figures 4a and 4b show the comparison of the computed Mach number contours with experimentally obtained schlieren photographs of the base

9

region flow field for I = 0 (no bleed) and I = .01, respectively. Both the experiment and the computed results show the flow expansion at the base corner and the recompression shock downstream of the base (coalescence of contour lines). In addition, Figures 4a and 4b show the free shear layer in the near wake. Although not indicated in Figure 4a, the flow in the near wake is primarily subsonic. For the zero bleed case, usual wake narrowing down (neck) can be clearly seen in both experimental and computational results. This is followed by a strong recompression shock wave system. With base bleed, the expansion at the base weakens, the shear layer angle is decreased, and the recompression shock is very weak. The widening of the wake with injection (I = .01) seen experimentally can also be observed in the computed results. The recirculatory flow field in the near wake for the zero bleed case gets displaced downstream. The computed results shown in Figure 4 were obtained using the two-equation k-ε model and the original grid.

Figure 5 shows the velocity profiles at the base bleed exit plane for various mass injection rates. The mass injection rates selected for the numerical computations were initially based on the experiment. However, experiment was rerun to provide detailed measurements in the near wake As it turned out, the injection rates obtained in the experimental data were slightly different from those used in the computation. Both computed and experimental results show the same trends. The exit velocity is quite uniform along the bleed exit. As expected, the magnitude of velocity increases with the increase in the mass injection rate. There is some discrepancy in velocity near the bleed orifice corner. This is due in part to the grid point distribution in this area. The grid points were not clustered in this region, since the flow inside the bleed hole, and thus, the boundary layer, is not modeled. The effect of base bleed on the mean axial velocity along the center line of symmetry is shown in Figure 6. The computed centerline velocity agrees fairly well with the experimental data in the near wake for x/D < 3.0. The agreement between the computed and experimental results is poor in the flow redevelopment region of the wake. This is true of all cases of mass injection rates. In both experiment and computed results, the bleed exit velocity is small for low injection rates and results in two stagnation points (forward and rear). The peak reverse velocity along the centerline decreases with the increase in base bleed rate. As mass injection rate is increased, the bleed exit velocity increases. The recirculation region in the near wake is reduced and pushed further downstream. For high injection rates (I =. 02 or higher), reverse velocity does not exist along the centerline. Figures 7 and 8 show the velocity components in the streamwise and normal directions, respectively, for a mass injection parameter of I = .01. These velocity profiles are taken at four longitudinal positions in the wake or the base region (X/D = 0.95, 1.26, 1.67, and 2.04). The stations

10

X/D = 0.95 and 1.67 correspond to the locations near the forward and rear stagnation points, respectively; X/D = 1.26 lies inside the recirculation region and X/D = 2.04 is in the flow redevelopment region downstream of the rear stagnation point. The computed velocity profiles obtained using the Baldwin-Lomax algebraic turbulence model and the two-equation k-ϵ model are compared with the experimental data. Figure 7 shows the comparison of the u (streamwise) component of velocity. In general, the profiles obtained with the k-ϵ model are in better agreement with the experiment in the shear layer regions for X/D = 0.95 and X/D = 1.26. The profiles are poorly predicted by the algebraic model at these two stations. At X/D = 0.95, both turbulence models predict reverse velocities near the centerline which are larger than the experimental value, although the k-ϵ model prediction is closer to the experiment. The predicted profiles near the centerline agree better with the experimental data further downstream (X/D = 1.26 and 1.67) inside the reverse flow region and near the rear stagnation point, especially the k-ϵ model prediction. Both models predict the velocity profiles at X/D = 1.67 and 2.04 fairly well. Figure 8 shows the comparison of the w (vertical) component of the velocity. This component of velocity is better predicted by the k-ϵ model than the algebraic model in the near wake, especially at X/D = 0.95. The profiles by the algebraic models are in poor agreement with the experimental data for radial positions greater than half of the base radius.

Some of the turbulence quantities are presented next. Figure 9 shows the turbulent kinetic energy profiles at the same longitudinal positions in the wake for the base bleed case, I =. 01. The computed k profiles are obtained using the two-equation k-ϵ turbulence model. Near the forward stagnation point (X/D = 0.95) and inside the separated flow region (X/D = 1.26), the peak observed experimentally is well predicted by the k-ϵ model. Some discrepancy exists between the computed results and the experimental data for r/R < 0.6. The agreement of the computed profiles, including the location and magnitude of the peak, with the data is much better near the rear stagnation point and downstream (X/D = 1.67 and 2.04), especially for the magnitude of the peak value. The location of the peaks decrease smoothly with increasing axial distances downstream from the base. Figure 10 shows the turbulent shear stress profiles in the near wake. The computed values obtained by both the algebraic model and the k-ϵ model are compared with the experimental data. In general, a small improvement can be observed in the predicted values with the k-ϵ model over the algebraic model. Discrepancy exists between the experimentally obtained turbulent shear stress and the predicted shear stresses with both turbulence models at X/D = 0.95 for r/R < 0.7. The location of the peak is better predicted by the k-ϵ model. The magnitude of the peak is well predicted by both

11

models. For the other stations in the near wake, the magnitude of the peaks is predicted well by both models. As for the location of the peak, the k-ε model does much better than the algebraic model. As X/D is increased from 0.95 to 2.04, the location of the peak predicted by the k-ε model moves closer to the center line similar to that observed in the experiment. This location of the peak is underpredicted by the algebraic model.

Of particular interest is the accurate prediction or determination of base pressure and, hence, base drag. Figure 11 shows the base pressure distribution (along the base) for a mass injection rate, I = .005. The base pressures predicted by both the algebraic model and the two-equation k-ε turbulence model are compared with the experimental data.[11] The experimental data are shown in dark circles, and the computed results are shown in lines. Here, Z/D = 0.0 corresponds to the center line of symmetry, and Z/D = 0.5 corresponds to the base corner. The base pressures predicted by both algebraic and k-ε turbulence models show almost no change in the base pressure distribution which can also be observed in the experimental data. The base pressure is, however, poorly predicted by the algebraic model. A much improved base pressure distribution is predicted by the k-ε model, and its agreement with the measured base pressure is quite good. The algebraic model prediction shows a slight variation near the base corner and the bleed exit corner. Figure 12 shows the base pressure distribution for an injection rate of I = 0.01. The computed base pressures obtained by both turbulence models are compared with the experimental data. Again the k-ε model predicted base pressure agrees well with the data, and the algebraic model prediction is poor. The grid sensitivity is examined in this figure using the results obtained by the k-ε model on three different grids (original medium, coarse, and fine). The coarse grid consists of half as many and the fine grid twice as many grid points as the original medium grid. The grid point distribution near the base also differs between these three grids. The y^+ values for these grids were .4, 1.4, and 8, respectively, for the fine, medium, and coarse grids. The difference in the computed base pressures obtained using the three grids is very small. This implies that the computed solution is grid independent, in at least as far as the base pressure is concerned. The base pressure comparison for a higher base bleed rate (I = 0.028) is shown in Figure 13. The three grids again have very similar results in base pressure with the k-ε model. The base pressure distribution for the k-ε model is shown here for the medium grid. The predicted base pressure with the k-ε model agrees better with the experimental data than that predicted by the algebraic model.

12

The effect of base bleed on base pressure is shown in Figure 14 as a function of mass injection parameter. The computed average base pressures predicted by both the algebraic and the k-ε model are compared with the experimental data. The algebraic turbulence model underpredicts the average base pressure for small mass injection rates. A much better average base pressure is predicted by the k-ε model, and its agreement with the measured average base pressure is quite good. The base pressure increases with the increase in the injection rate for low injection rates. This is the region where the base bleed is effective in increasing the base pressure and thereby reducing the base drag. The increase in base pressure with increasing injection rates occurs until the optimum bleed rate is reached. This optimum injection rate is approximately 0.015 as evidenced from the experimental data. The peak predicted by k-ε model agrees well the data. The peak predicted by the algebraic model is near 0.02 and is not in good agreement with the data. With further increase in the injection rate from its optimum, the base pressure decreases, as evidenced by both experimental data and computed results.

5. CONCLUDING REMARKS

A zonal, implicit, time-marching Navier-Stokes computational technique has been used to compute the turbulent supersonic base flow over a cylindrical afterbody with base bleed. Flow field computations have been performed at $M_\infty = 2.46$ and at a 0° angle of attack. Two eddy viscosity turbulence models (an algebraic and a two-equation k-ε) have been used to provide the turbulence closure. The k-ε equations are solved using an implicit algorithm, and calculations with the k-ε model are extended up to the wall.

Numerical results show the details of the flow field in terms of Mach number contours. Comparison of both the mean and turbulence quantities have been made with the available experimental data. The algebraic turbulence model predicts the mean velocity components poorly in the wake. In general, the velocity components predicted by the two-equation k-ε model are in better agreement with the experimental data than the algebraic model. Small discrepancy exists between the predicted turbulent shear stress and the experiment for both algebraic and k-ε turbulence models. An improvement in the predicted location and magnitude of the peak in shear stress is found with the k-ε model. Computed base pressure distributions have been compared with the measured base pressures. The base pressures are underpredicted by the algebraic model for

13

different injection rates. The predicted base pressures for these injection rates with the k-ε model are found to be in good agreement with the experimental measured base pressures.
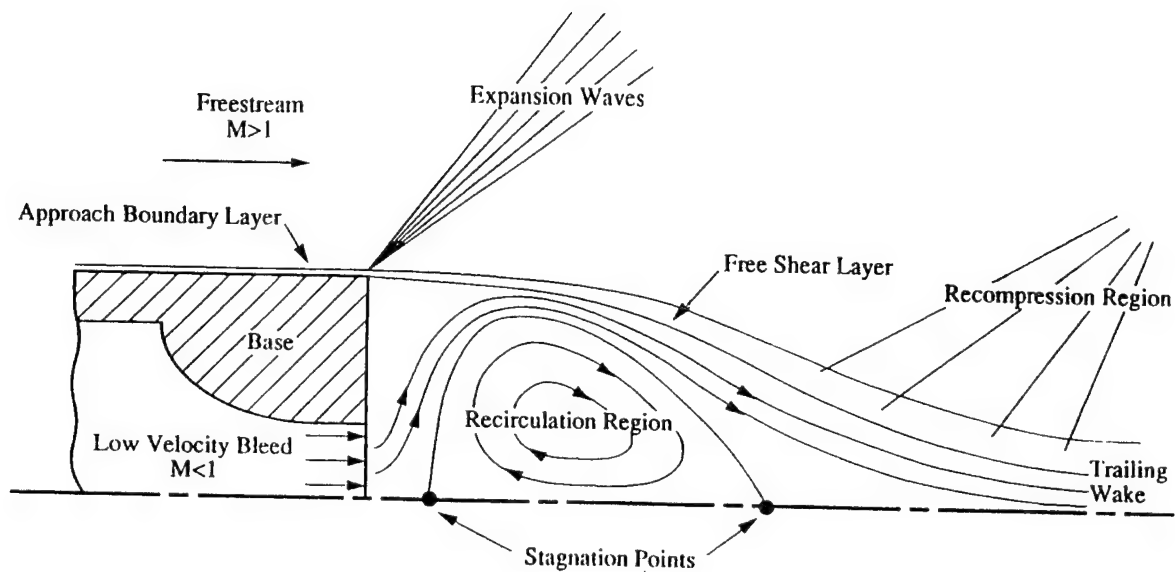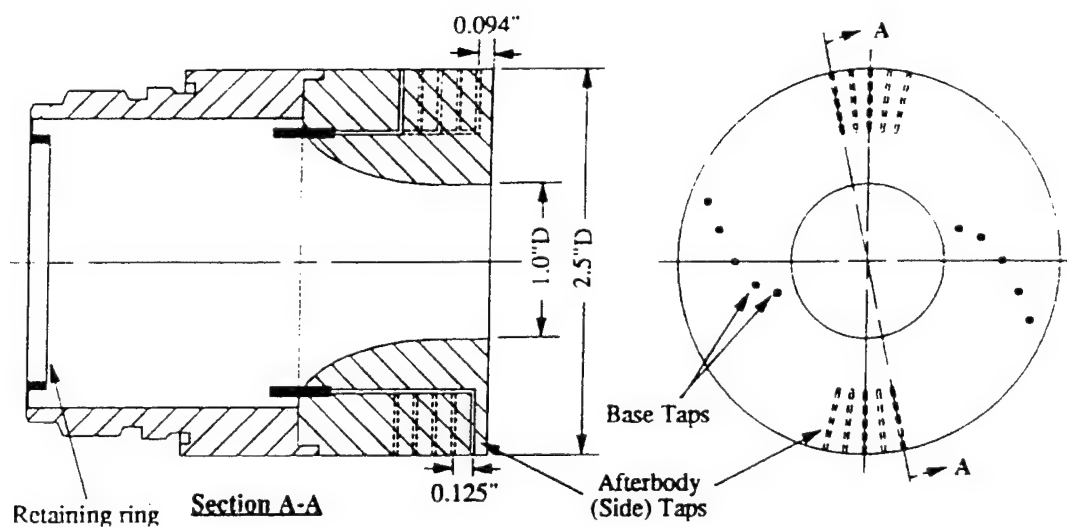
Figure 1. Schematic Diagram of Supersonic Base Flow.

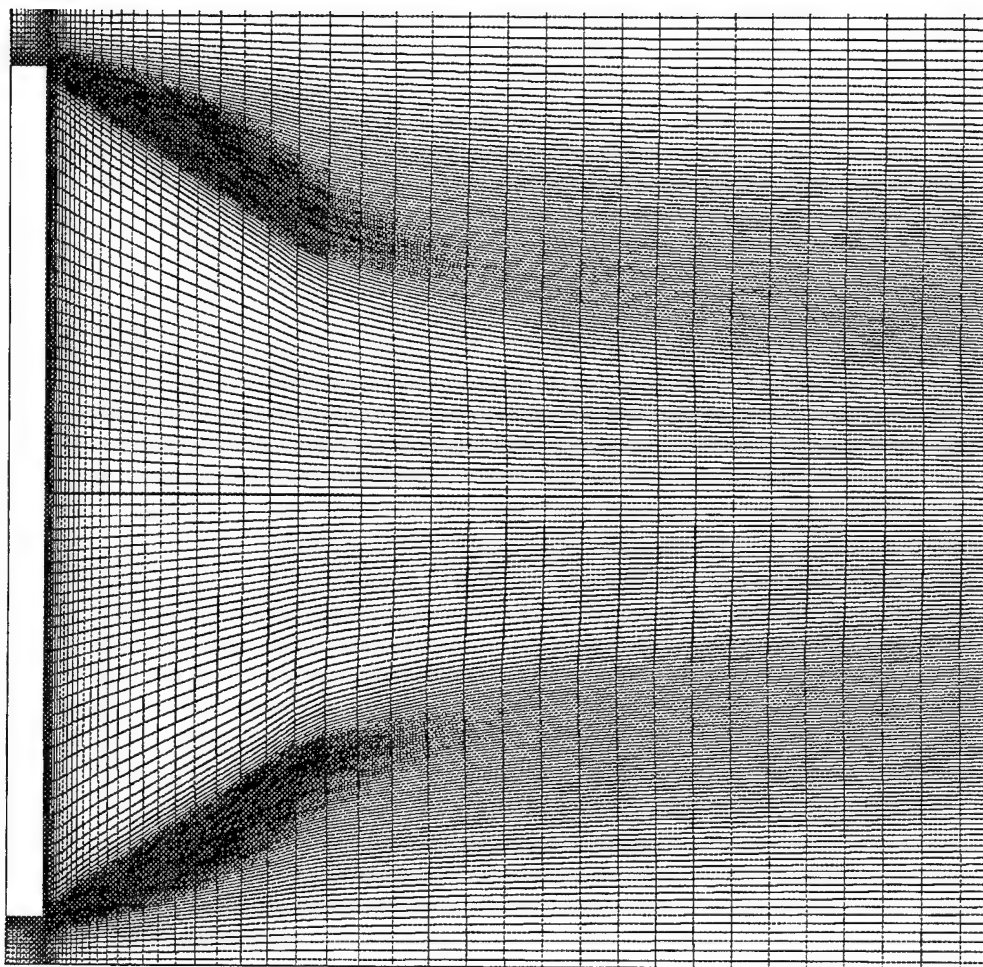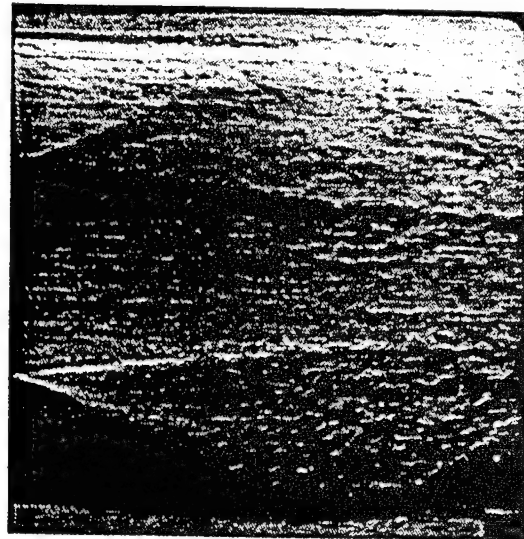Figure 2. Afterbody Measurement Locations.
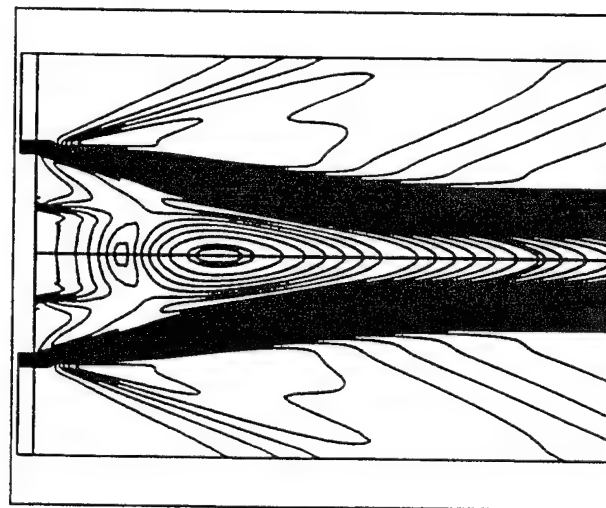
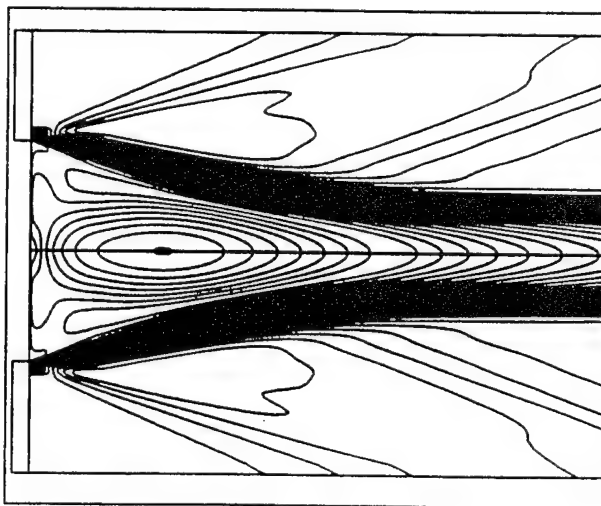Figure 3. Base Region Computational Grid.

(a)

(b)

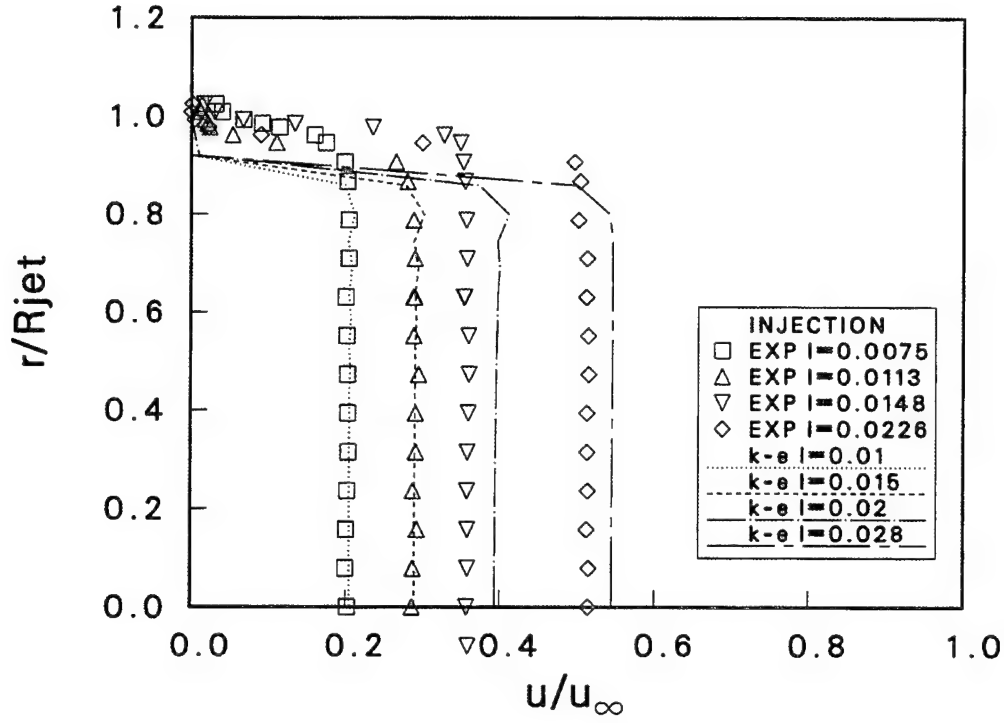Figure 4. Computed Mach Contours and Experimental Schlieren Photograph, $M_\infty = 2.46$, $\alpha = 0$, a) $I = 0.0$, b) $I = 0.01$.

Figure 5. Mean Axial Velocity Distributions at Bleed Exit, $M_\infty = 2.46$, $\alpha = 0$, and k-ε Model.
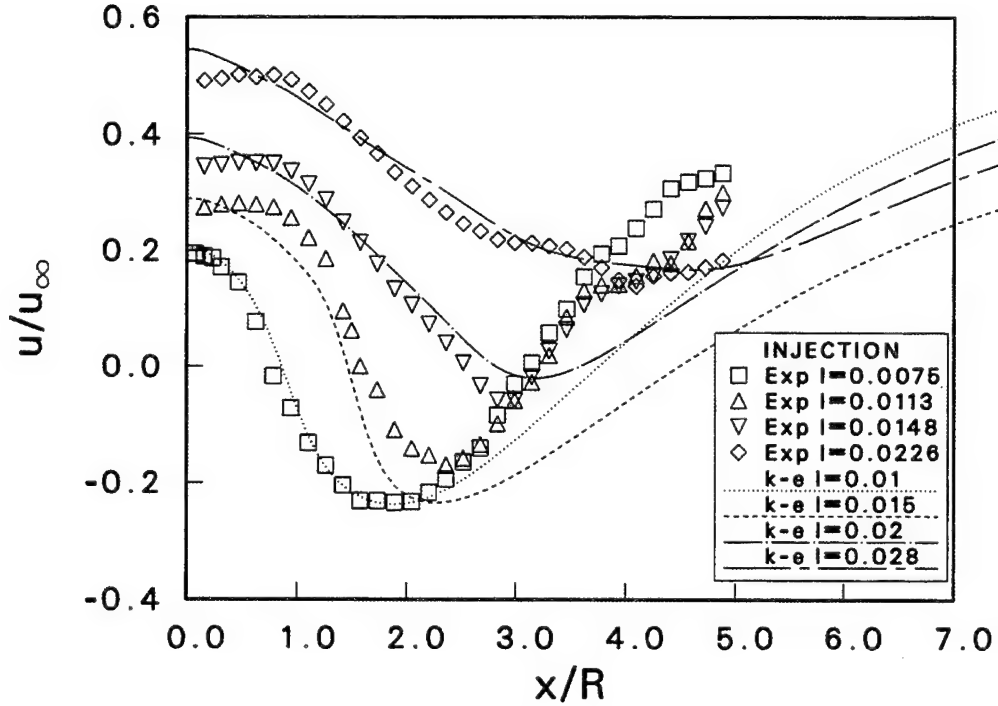
Figure 6. Mean Axial Velocity along the Centerline, $M_\infty = 2.46$, $\alpha = 0$, and k-ε Model.
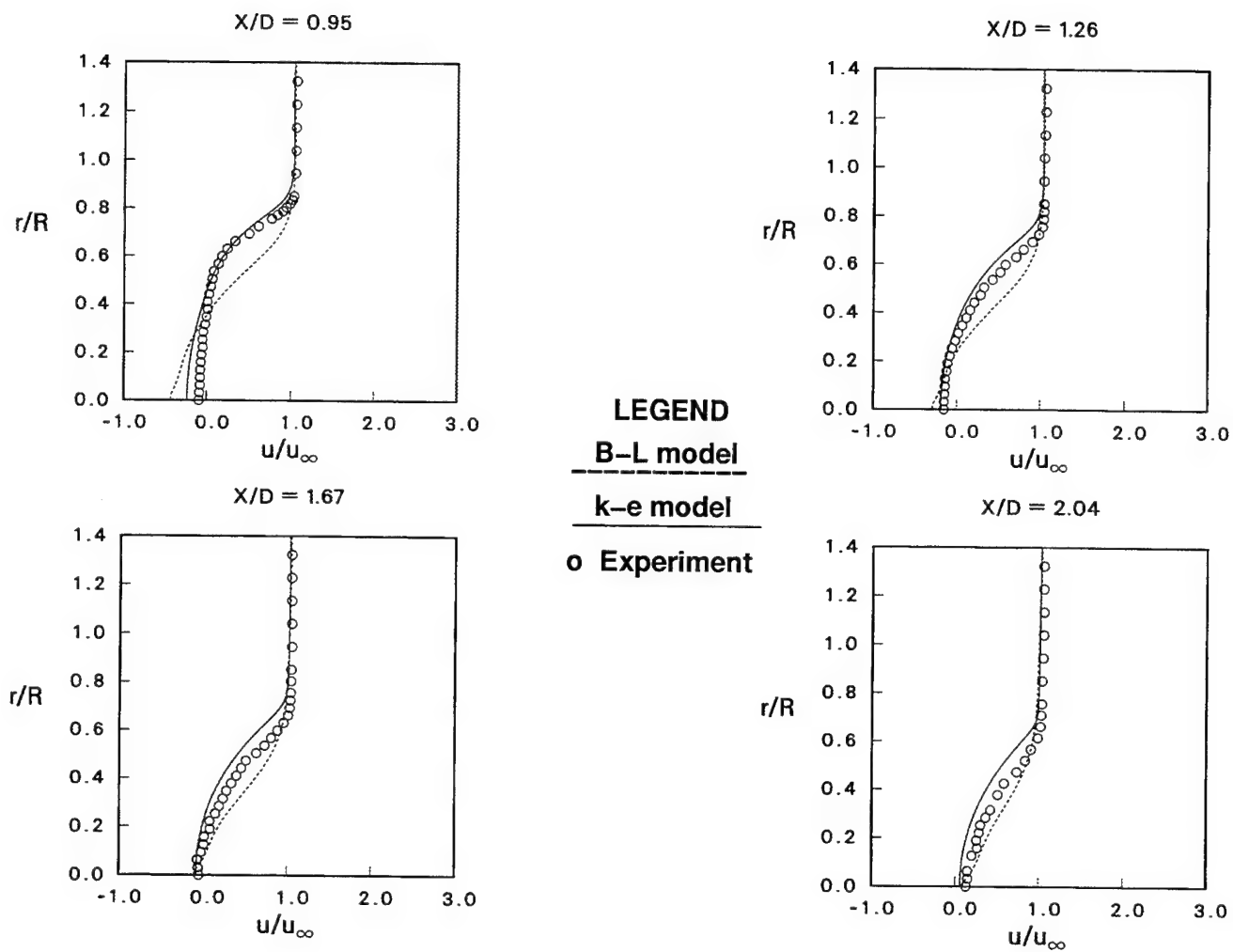
Figure 7. <u>Streamwise Velocity (u) Profiles, $M_\infty = 2.46$, $\alpha = 0$, $I = 0.01$.</u>
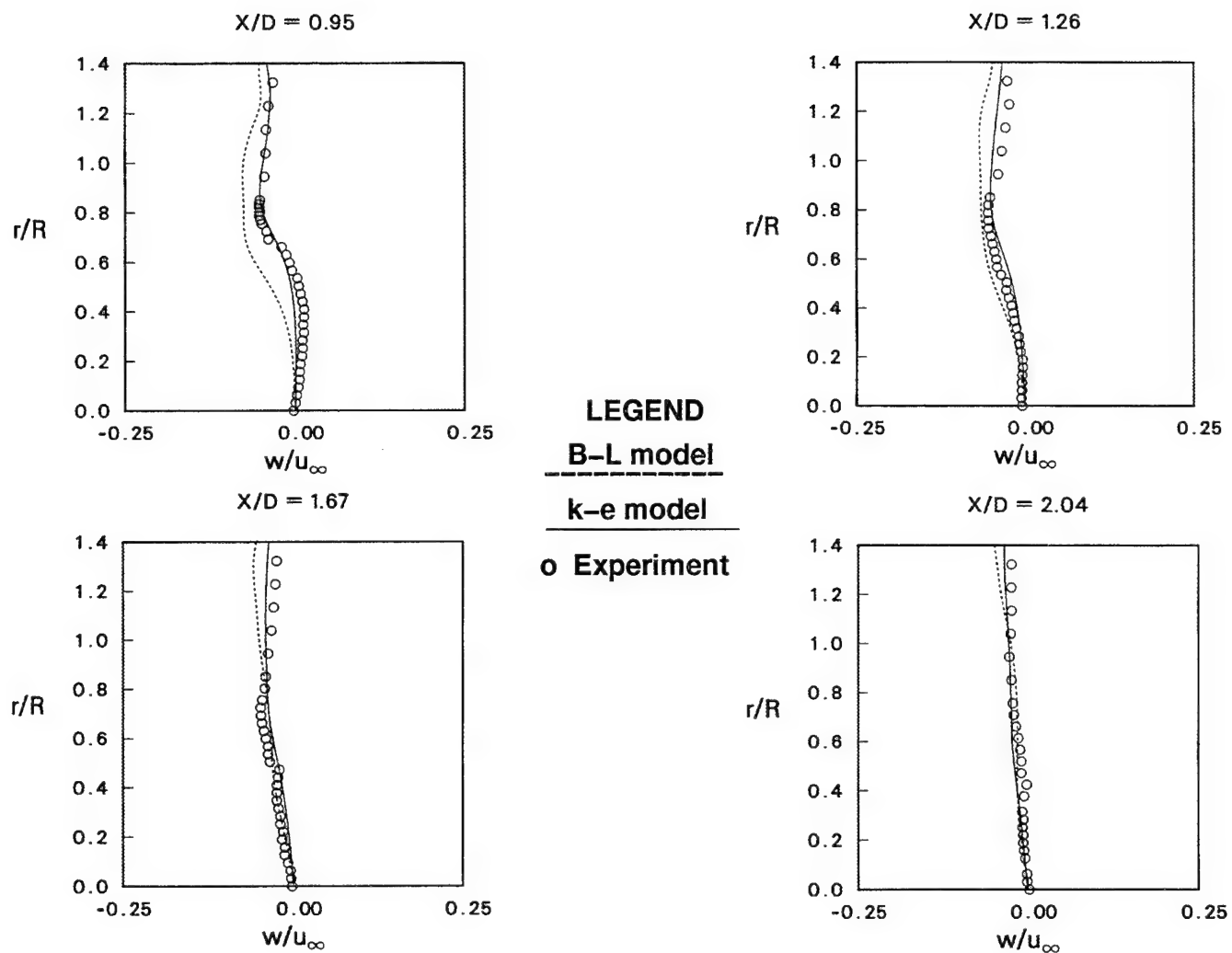
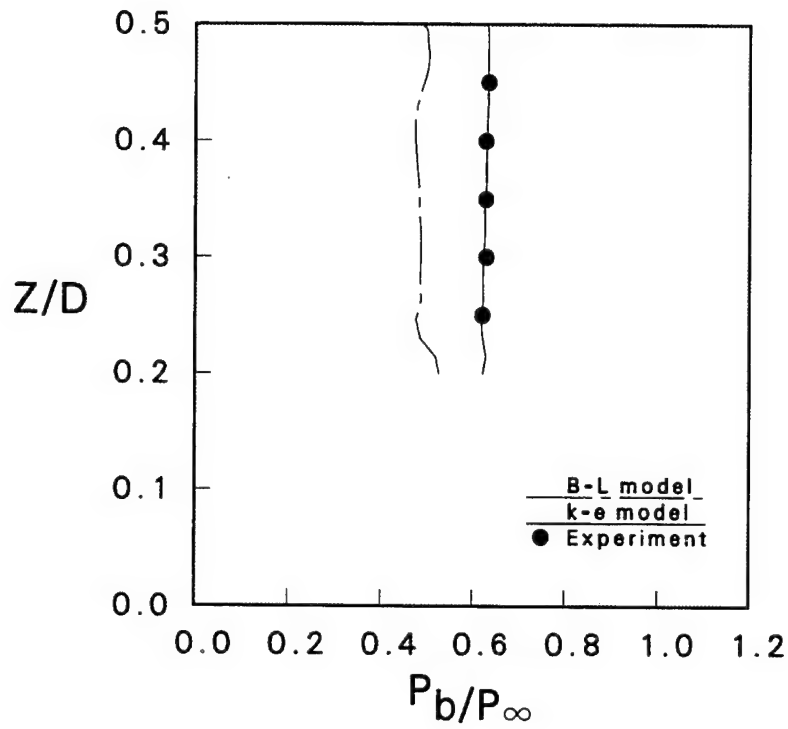Figure 8. Normal Velocity (w) Profiles, $M_\infty = 2.46$, $\alpha = 0$, $l = 0.01$.
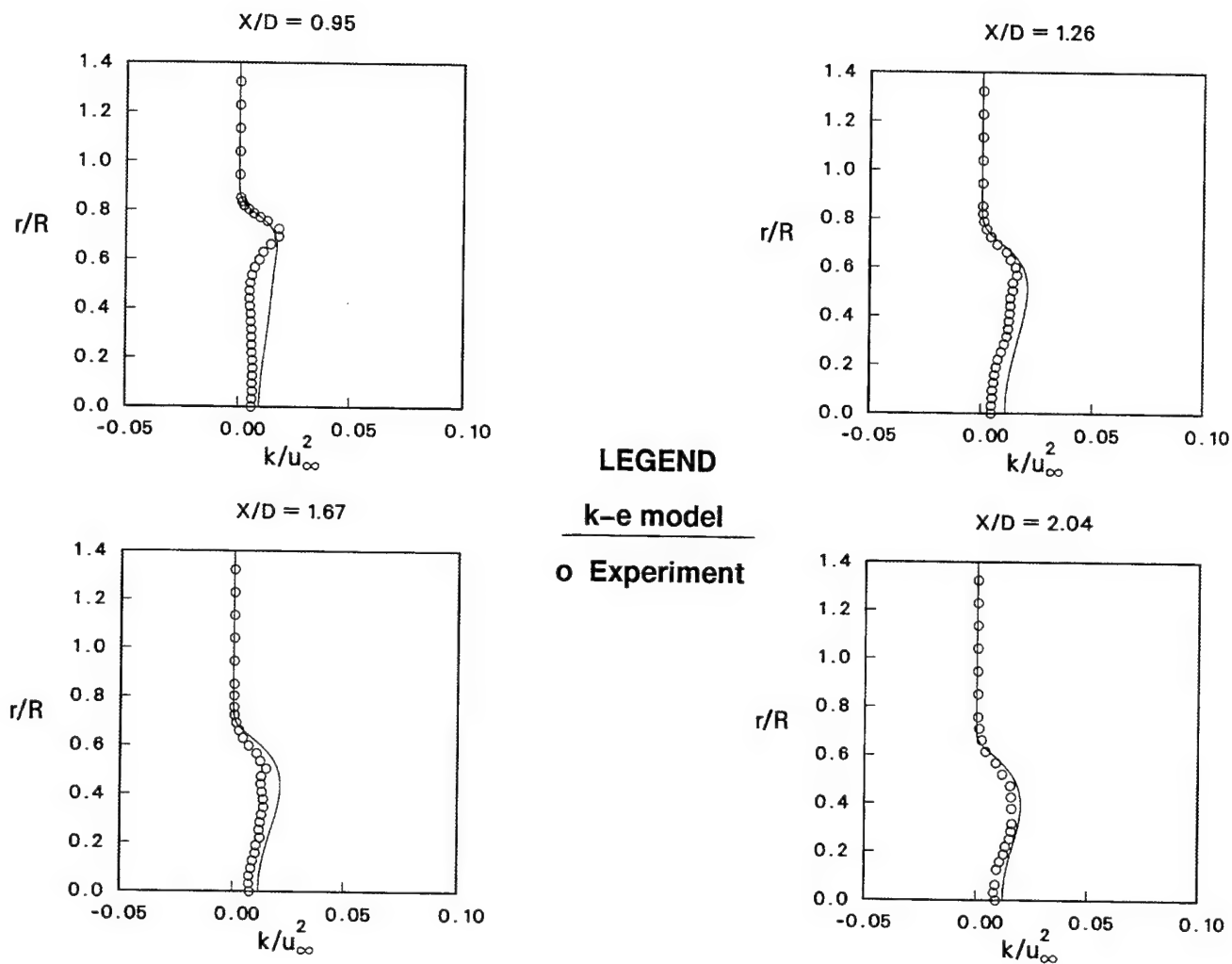
Figure 9. Turbulent Kinetic Energy Profiles, $M_\infty = 2.46$, $\alpha = 0$, $I = 0.01$.

21
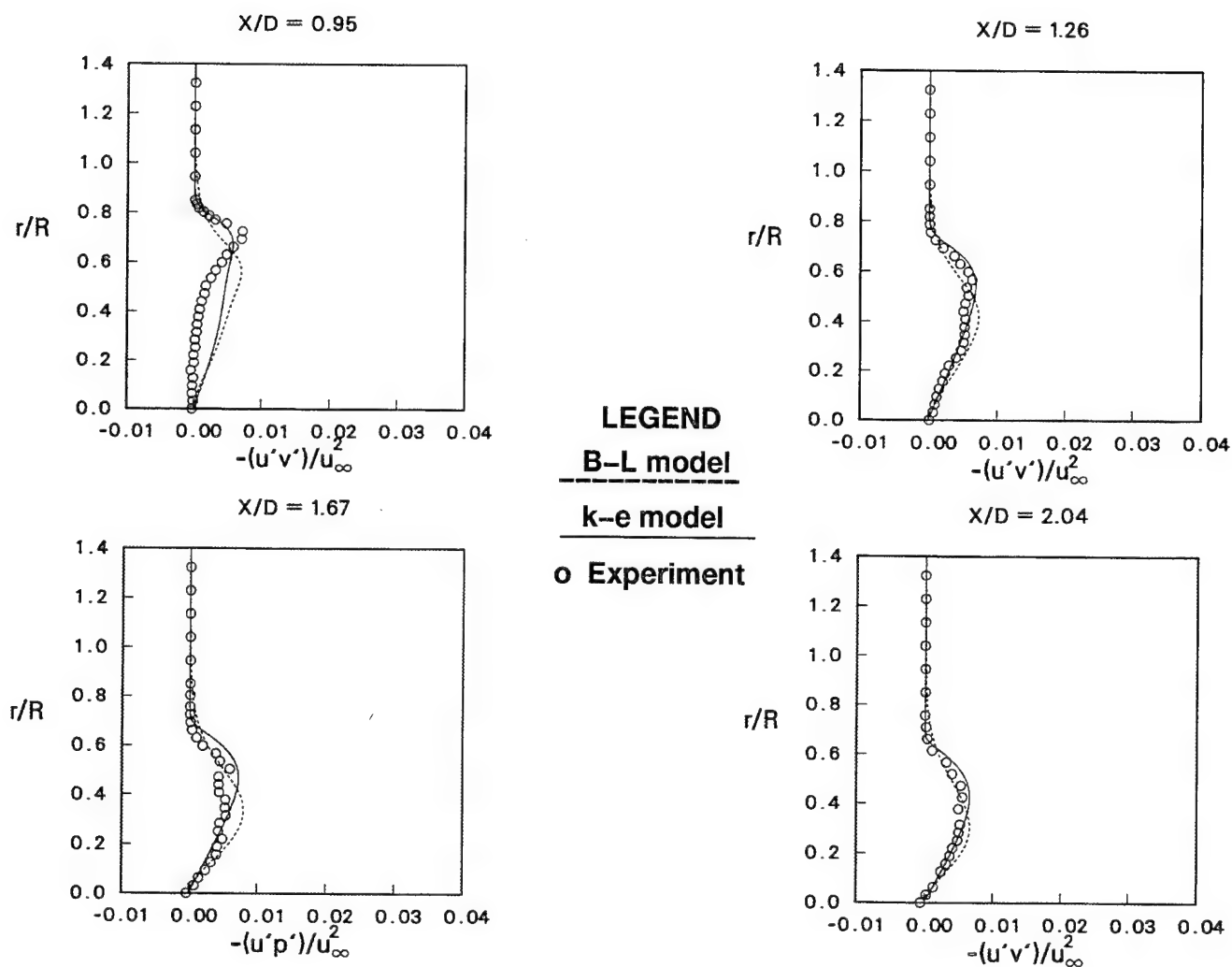
Figure 10. Turbulent Shear Stress Profiles, $M_\infty = 2.46$, $\alpha = 0$, $I = 0.01$.

22

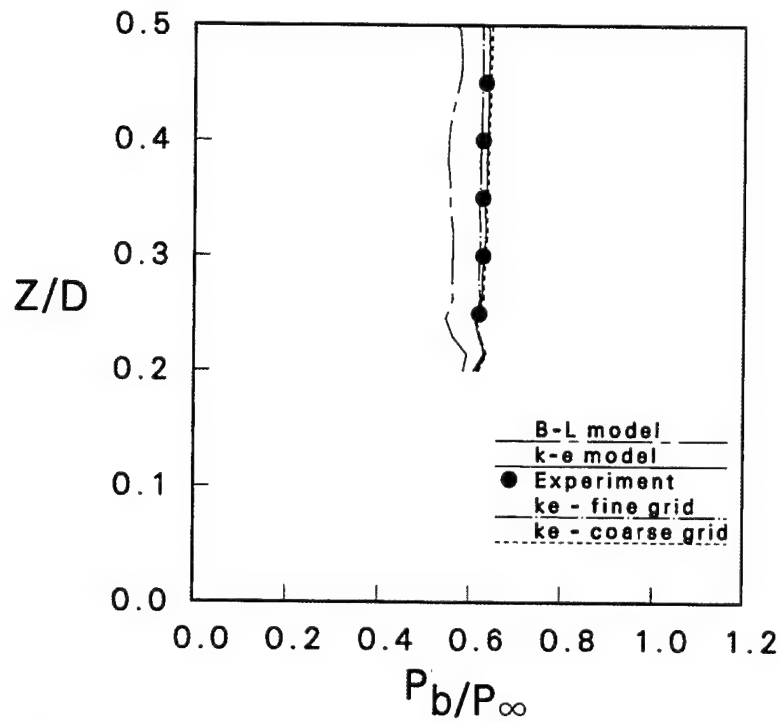Figure 11. Base Pressure Distribution, M$_\infty$ = 2.46, α = 0, I = 0.005.

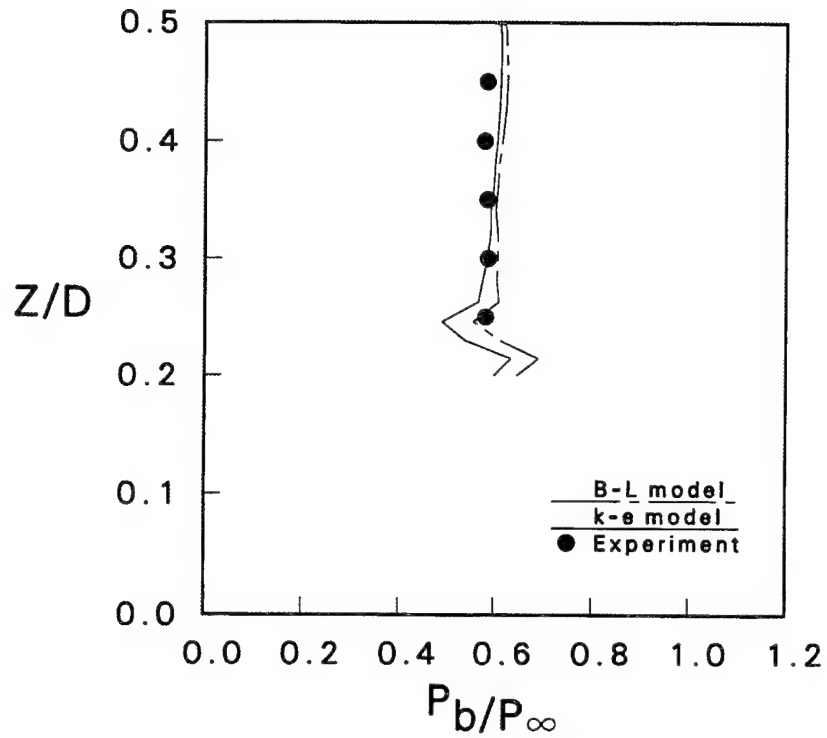Figure 12. Base Pressure Distribution, M$_\infty$ = 2.46, α = 0, I = 0.01.

23

Figure 13. Base Pressure Distribution, M_∞ = 2.46, α = 0, I = 0.028.
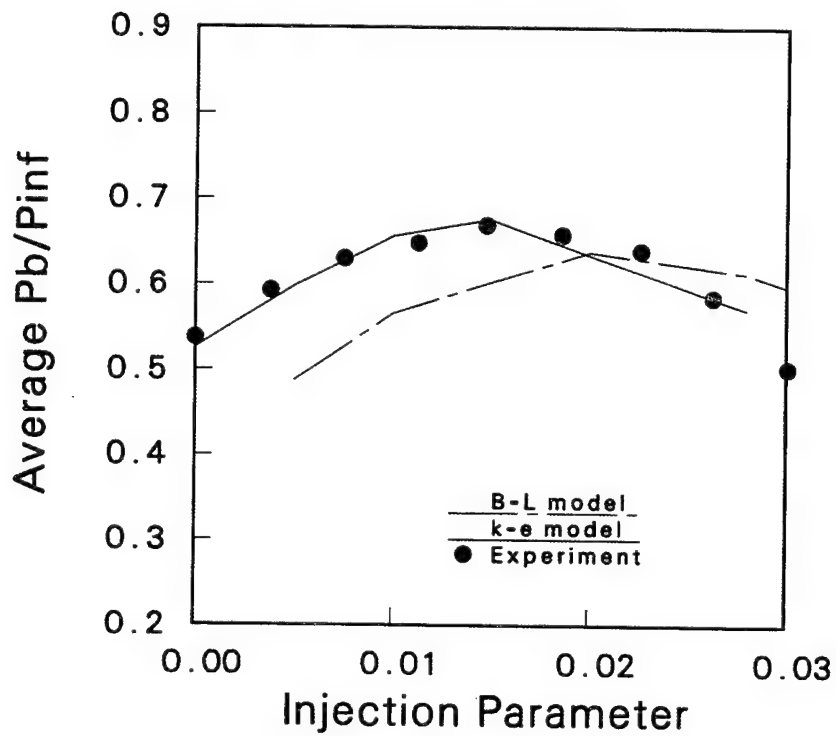
Figure 14. Effect of Base Bleed on Average Base Pressure, M_∞ = 2.46, α = 0.

24

6. REFERENCES

1. Sahu, J., C. J. Nietubicz, and J. L. Steger. "Navier-Stokes Computations of Projectile Base Flow With and Without Base Injection." BRL-TR-02532, U.S. Army Ballistic Research Laboratory, Aberdeen Proving Ground, MD, November 1983 (also see AIAA Journal, vol. 23, no. 9, pp. 1348–1355, September 1985).

2. Sahu, J. "Supersonic Base Flow Over Cylindrical Afterbodies With Base Bleed." AIAA Paper No. 86-0487, Proceedings of the 24th Annual Aerospace Sciences Meeting, Reno, NV, January 1986.

3. Sahu, J. "Computations of Supersonic Flow Over a Missile Afterbody Containing an Exhaust Jet." AIAA Journal of Spacecraft and Rockets, vol. 24, no. 5, pp. 403–410, September–October 1987.

4. Sahu, J. "Numerical Computations of Transonic Critical Aerodynamic Behavior." AIAA Journal, vol. 28, no. 5, pp. 807–816, May 1990 (also see BRL-TR-2962, December 1988).

5. Sahu, J., and C. J. Nietubicz. "Three Dimensional Flow Calculation for a Projectile With Standard and Dome Bases." BRL-TR-3150, U.S. Army Ballistic Research Laboratory, Aberdeen Proving Ground, MD, September 1990.

6. Herrin, J. L., and J. C. Dutton. "Supersonic Base Flow Experiments in the Near-Wake of a Cylindrical Afterbody." AIAA Journal, vol. 32, no. 1, pp. 77–83, 1994.

7. Sahu, J. "Numerical Computations of Supersonic Base Flow With Special Emphasis on Turbulence Modeling." AIAA Journal, vol. 32, no. 7, July 1994.

8. Bowman, J. E., and W. A. Clayden. "Cylindrical Afterbodies in Supersonic Flow With Gas Ejection." AIAA Journal, vol. 5, no. 8, pp. 1524–1525, August 1967.

9. Clayden, W. A., and J. E. Bowman. "Cylindrical Afterbodies at $M_\infty = 2$ With Hot Gas Ejection." AIAA Journal, vol. 6, no. 12, pp. 2429–2431, December 1968.

10. Schilling, H. "Experimental Investigation on the Base-bleed-Effect for Boat-Tail-Combinations." Proceedings of the 8th International Symposium on Ballistics, Amsterdam, Holland, 1984.

11. Mathur, T., and J. C. Dutton. "Base Bleed Experiments With a Cylindrical Afterbody in Supersonic Flow." AIAA Paper No. 95-0062, January 1995.

12. Pulliam, T. H., and J. L. Steger. "On Implicit Finite-Difference Simulations of Three-Dimensional Flow." AIAA Journal, vol. 18, no. 2, pp. 159–167, February 1982.

13. Baldwin, B. S., and H. Lomax. "Thin Layer Approximation and Algebraic Model for Separated Turbulent Flows." AIAA Paper No. 78-257, January 1978.

14. Chien, K. Y. "Predictions of Channel and Boundary-Layer Flows With a Low-Reynolds-Number Turbulence Model." AIAA Journal, vol. 20, pp. 33–38, January 1982.

15. Jones, W. P., and B. E. Launder. "The Prediction of Laminarization With a Two-Equation Model of Turbulence." International Journal of Heat and Mass Transfer, vol. 15, 1972.

16. Sahu, J., and J. E. Danberg. "Navier-Stokes Computations of Transonic Flows With a Two-Equation Turbulence Model." AIAA Journal, vol. 24, no. 11, pp. 1744–1751, November 1986.

NO. OF
COPIES   ORGANIZATION

2   DEFENSE TECHNICAL INFO CTR
    ATTN DTIC DDA
    8725 JOHN J KINGMAN RD
    STE 0944
    FT BELVOIR VA 22060-6218

1   DIRECTOR
    US ARMY RESEARCH LAB
    ATTN AMSRL OP SD TA
    2800 POWDER MILL RD
    ADELPHI MD 20783-1145

3   DIRECTOR
    US ARMY RESEARCH LAB
    ATTN AMSRL OP SD TL
    2800 POWDER MILL RD
    ADELPHI MD 20783-1145

1   DIRECTOR
    US ARMY RESEARCH LAB
    ATTN AMSRL OP SD TP
    2800 POWDER MILL RD
    ADELPHI MD 20783-1145

    ABERDEEN PROVING GROUND

5   DIR USARL
    ATTN AMSRL OP AP L (305)

27

1   HQDA
ATTN SARD TR
MS K KOMINOS
WASHINGTON DC 20310-0103

1   HQDA
ATTN SARD TR
DR R CHAIT
WASHINGTON DC 20310-0103

2   USAF WRIGHT AERONAUTICAL
LABORATORIES
ATTN AFWAL FIMG
DR J SHANG
MR N E SCAGGS
WPAFB OH 45433-6553

3   COMMANDER
NAVAL SURFACE WEAPONS CNTR
ATTN CODE R44 DR F PRIOLO
CODE R44 DR A WARDLAW
K24 B402 12 DR W YANTA
WHITE OAK LABORATORY
SILVER SPRING MD 20903-5000

4   DIRECTOR
NATIONAL AERONAUTICS AND
SPACE ADMINISTRATION
LANGLEY RESEARCH CENTER
ATTN TECH LIBRARY
MR D M BUSHNELL
DR M J HEMSCH
DR J SOUTH
LANGLEY STATION
HAMPTON VA 23665

2   INTERFEROMETRICS INC
8150 LEESBURG PIKE
ATTN RENE LARRIVA
ERIC L STROBEL
VIENNA VA 22180

2   ARPA
ATTN DR P KEMMEY
DR JAMES RICHARDSON
3701 NORTH FAIRFAX DR
ARLINGTON VA 22203-1714

6   DIRECTOR
NASA
AMES RESEARCH CENTER
ATTN MS 227 8 L SCHIFF
MS 258 1 T HOLST
MS 258 1 D CHAUSSEE
MS 258 1 M RAI
MS 258 1 P KUTLER
MS 258 1 P BUNING
MOFFETT FIELD CA 94035

1   USMA
DEPT OF MECHANICS
ATTN LTC ANDREW L DULL
WEST POINT NY 10996

6   COMMANDER
US ARMY ARDEC
ATTN SMCAR AET A
R DEKLEINE
C NG
R BOTTICELLI
H HUDGINS
J GRAU
S KAHN
PICATINNY ARSENAL NJ 07806-5001

1   COMMANDER
US ARMY ARDEC
ATTN SMCAR CCH V
PAUL VALENTI
PICATINNY ARSENAL NJ 07806-5001

1   COMMANDER
US NAVAL SURFACE WEAPONS CTR
ATTN DR F MOORE
DAHLGREN VA 22448

3   UNIV OF CALIFORNIA DAVIS
DEPT OF MECHANICAL ENGG
ATTN PROF H A DWYER
PROF M HAFEZ
DR B MEAKIN
DAVIS CA 95616

No. of
Copies   Organization

1   UNIVERSITY OF FLORIDA
         DEPT OF ENGG SCIENCES
         COLLEGE OF ENGINEERING
         ATTN   PROF C C HSU
         GAINESVILLE FL 32611

         ABERDEEN PROVING GROUND

25   DIR USARL
         ATTN   AMSRL-WT-P
                    MR ALBERT HORST
                AMSRL-WT-PB
                   DR E SCHMIDT
                   DR M BUNDY
                   DR K FANSLER
                   MR E FERRY
                   MR B GUIDOS
                   MRS K HEAVEY
                   MR H EDGE
                   MR V OSKAY
                   DR P PLOSTINS
                   DR A MIKHAIL
                   DR J SAHU
                   MR P WEINACHT
                AMSRL-WT
                   DR J ROCCHIO
                AMSRL-WT-PD
                   DR B BURNS
                AMSRL-WT-PA
                   DR T MINOR
                   MR M NUSCA
                AMSRL-WT-PC
                   DR R FIFER
                AMSRL-WT-W
                   DR C MURPHY
                AMSRL-WT-WB
                   DR W D'AMICO
                AMSRL-WT-NC
                   MR R LOTTERO
                AMSRL-CI-C
                   DR W STUREK
                AMSRL-SC-C
                   MR C NIETUBICZ
                   MS D HISLEY
                AMSRL-SL-C
                   M MILLER

2   CDR ARDEC
         ATTN   FIRING TABLES, BLDG 120
                    MR R LIESKE

30

USER EVALUATION SHEET/CHANGE OF ADDRESS

This Laboratory undertakes a continuing effort to improve the quality of the reports it publishes. Your comments/answers to the items/questions below will aid us in our efforts.

1. ARL Report Number ___ARL-TR-955_____ Date of Report ___December 1995_____

2. Date Report Received _____

3. Does this report satisfy a need? (Comment on purpose, related project, or other area of interest for which the report will be used.) _____

_____

_____

4. Specifically, how is the report being used? (Information source, design data, procedure, source of ideas, etc.) _____

_____

_____

5. Has the information in this report led to any quantitative savings as far as man-hours or dollars saved, operating costs avoided, or efficiencies achieved, etc? If so, please elaborate. _____

_____

_____

6. General Comments. What do you think should be changed to improve future reports? (Indicate changes to organization, technical content, format, etc.) _____

_____

_____

_____

	Organization
CURRENT ADDRESS	Name
	Street or P.O. Box No.
	City, State, Zip Code

7. If indicating a Change of Address or Address Correction, please provide the Current or Correct address above and the Old or Incorrect address below.

	Organization
OLD ADDRESS	Name
	Street or P.O. Box No.
	City, State, Zip Code

(Remove this sheet, fold as indicated, tape closed, and mail.)
(DO NOT STAPLE)

DEPARTMENT OF THE ARMY

OFFICIAL BUSINESS

BUSINESS REPLY MAIL
FIRST CLASS PERMIT NO 0001,APG,MD

POSTAGE WILL BE PAID BY ADDRESSEE

DIRECTOR
U.S. ARMY RESEARCH LABORATORY
ATTN: AMSRL-WT-PB
ABERDEEN PROVING GROUND, MD 21005-5066